Remarkable piezoelectric properties in thin films of cellulose nanofibers after electrochemical poling

Ayesha Sultana
Linköping University
Md. Mehebub Alam
Linköping University
Eleni Pavlopoulou
University of Bordeaux https://orcid.org/0000-0002-5291-0132
Eduardo Solano
NCD-SWEET beamline, ALBA synchrotron light source https://orcid.org/0000-0002-2348-2271
Magnus Berggren
Linköping University https://orcid.org/0000-0001-5154-0291
Xavier Crispin (xavier.crispin@liu.se)
Linköping University https://orcid.org/0000-0001-8845-6296
Dan Zhao
Linköping University https://orcid.org/0000-0001-5266-6726

Article

Keywords:

Posted Date: December 22nd, 2021

DOI: https://doi.org/10.21203/rs.3.rs-1134434/v1

Abstract

Internet-of-everything (IoE) is defined as networked connections of things, people, data and processes. IoE nodes, preferably shaped as printed flexible systems, serves as the frontier outpost of the Internet and comprises devices to record and regulate states and functions. To power distributed IoE nodes in an ecofriendly manner, technology to scavenge energy from ambience and self-powered devices are developed. For this, piezoelectricity is regarded as a key-property, however current technology typically based on polyvinylidene difluoride (PVDF) co-polymers, are expensive and produced via toxic protocols.

We report piezoelectric characteristics of electrochemically poled cellulose nanofiber (CNFs) thin films processed from water dispersions. Poling these films at humid conditions cause breaking and reorientation of CNF segments, which results in enhanced crystal alignment rendering the resulting material piezoelectric. Generators based on poled CNF show similar piezoelectric voltage and coefficient, here measured to d_{33} = 46 pm/V, as for devices including PVDF copolymer layers of similar thickness. Our findings promise for low cost and printable ecofriendly piezoelectric-powered IoE nodes.

Introduction

Internet-of-Everything (IoE) [1] is currently one of the strongest tech-trends with many great applications already in operation and a vast array of opportunities forecasted. To settle this technology as an ecofriendly technology, we need to make sure that all included materials are derived from sustainable origins and that they are processed and recycled under protocols with a minimal impact on the environment [2]. To power and to integrate self-powered devices into IoE nodes, various properties and functions are being explored to enable heavily distributed and remote autarchic nodes within future Fog Computing systems [3]. In this respect, piezoelectric materials have been widely applied in energy harvesting and signal transducing applications.

Piezoelectric materials couple mechanical stress, such as displacement, pressure, vibration and flows to electrical polarization [4, 5], which have been used for powering portable electronic devices and wireless sensors [6, 7] as well as in actuators and acoustic devices [8]. The strength of the mechano-to-electric coupling described as the piezoelectric coefficient is defined as the ratio between the generated charge and the applied mechanical force [9]. In recent decades, piezoelectric polymers have become the focus because of the possibility to use atmospheric synthetic routes as well as the ability to make flexible thin films by solution processing, such as printing technologies, despite their typically lower piezoelectric coefficient compared to inorganics [10]. The best-performing piezoelectric polymers are fluoropolymers based on polyvinylidene difluoride (PVDF) and its copolymer P(VDF-TrFE) (polyvinylidene fluoride trifluoroethylene). Recently, a high piezoelectric coefficient of 52 p CN^{-1} was reported for P(VDF-TrFE) composited with Mxene nanosheets [11]. With the awareness of the human footprint on the environment, IoE applications imply massive number of small devices released in society and nature. Here, the fluorine chemistry and the release of HF toxic fume upon thermal degradation of the PVDF material are issues for chemical synthesis and recyclability [12]. Hence, a new generation of green piezoelectric materials,

comprising features such as low cost, water solution processibility, and an overall environmental friendliness is in urgent need. So far, the highest piezoelectric coefficient found in biomaterials reaches 38 pC N^{-1} at nanoscale characterized by piezoresponse force microscopy (PFM) [13]. Although this high value was not correlated to piezoelectric devices of practically large area, it showed the potential of biomaterials for piezoelectricity.

As the most abundant and green material on earth, cellulose-based materials have triggered a tremendous research attention over the last decades. The piezoelectricity in wood was discovered already in 1950 [14], followed by explanation that the origin of shear piezoelectricity is correlated to the reorientation of dipole moment from hydroxyl groups in the crystalline cellulose [15]. The intra- and inter molecular hydrogen bonds along the side of the cellulose chain introduce a non-centrosymmetric crystal structure in cellulose [16, 17]. The piezoelectric coefficients of those bulk wood-based materials are very low, which hinders their practical applications [18]. More recent, the topic went through a phase of renaissance thanks to the exploration of nanocelluloses that opened up new possibilities to make cellulose material systems with unique properties. Cellulose nanocrystals (CNCs) of diameter between 5-20 nm and a length of about 100-500 nm are the smallest crystalline features extracted from wood via mechanical and chemical treatments. Cellulose nanofibers (CNFs) can be several micrometers long with amorphous and crystalline domains (mentioned as CNC) arranged alternatively.

For a single cellulose crystal, apart from the shear piezoelectric constants, longitudinal and transverse piezoelectric constants are also present [19–21] because of the permanent dipole moment along their axis [22]. The longitudinal piezoelectric coefficient d_{33} enables the most promising applications because maximum deformation occurs when the output voltage and the applied mechanical strain are in the same direction. Orienting randomly arranged CNC to aligned structure in a particular direction could increase the piezoelectric constant. However, most of the reported methods only succeeded to align CNFs and CNCs parallel to the substrate [20, 23, 24]; thus not leading to any virtual enhancement of d_{33}. The difficulty to orient the nanocellulose homogeneously across large area and the extreme fragility of the CNCs films prevent cellulose to be implemented in efficient and high-performing piezoelectric devices [21]. The practical piezoelectric devices composed of nanocellulose only exhibit a low piezoelectric constant (5 pC N^{-1}), that is 4-5 times smaller than ones based on PVDFs [19]. Till now there is no research showing that pure cellulose can exhibit competitive piezoelectric performance compared to PVDF derivatives in practical devices.

In this work, we report that electrochemical poling greatly enhances the piezoelectric property of CNF thin films, which can be implemented in macroscopic devices (area of about 1 cm^2) to exhibit competitive performance with P(VDF-TrFE)-based piezoelectric devices of similar thickness. Different from the electric poling process used to polarize typical ferroelectric materials to improve piezoelectricity, the proposed electrochemical poling mechanism involves absorbed water from air, breaking and reorientation of the CNF under electrochemical reactions. Atomic force microscopy (AFM) was here used to reveal the role of humidity and visualizes the changes of CNF thin film morphology after electrochemical poling. The

mechanism is supported by impedance spectroscopy and grazing-incidence small-angle X-ray scattering (GISAXS) characterization of the CNF films before and after poling. We also confirmed the improved d_{33} piezoelectric coefficient of CNF thin films and measures values reaching up to 46 pm V^{-1} using PFM, which is comparable to P(VDF-TrFE) (45 pm V^{-1}). Our work demonstrates the possibility of nanocellulose to compete with PVDF copolymers processed from solution. Our findings pave the way for ecofriendly novel all-printed energy technology and sensors for IoE application in general and may also find its way into some niche-application for large area energy harvesting systems.

Results

Piezoelectric voltage of CNF thin films

The CNF thin films were prepared on doped silicon wafers by drop-casting a fixed amount of water dispersion of CNF with 0.5 wt% solid content (Fig. 1a). The conductive silicon wafer and the top Au electrode were connected to form a close circuit for both electric poling and piezoelectric characterizations (Fig. 1b). The photograph and dimension of a result device is shown in the inset figure in Fig. 1c. The CNF film was poled with gradually increasing voltage from 5 V to 110 V. After each voltage step, the piezoelectric response of the same film was recorded while applying the same force. Fig. 1c presents the piezoelectric performance for a Si/CNF/Au device at ambient humidity (RH=40%). Those traces correspond to the open circuit piezoelectric output voltage upon a periodic applied force (24 N) at frequency of 3 Hz. There is no obvious piezoelectric response above the non-periodical noise level (<10 mV) for the device before poling. For poling voltages below 30 V, a periodic output voltage following the 3Hz input force is observed with an amplitude of around 30 mV. Above 30 V, the piezoelectric voltage increases and reaches a maximum of 100 mV at a poling voltage of 70 V. For poling voltages higher than 70 V, there is a degradation of the performance with a slight decrease in output voltage. We also tested the piezoelectric response of the same device 30 minutes after poling (with the same force F=24 N), see Fig. 1c, there is no obvious degradation of the output voltage. The asymmetry between positive and negative voltage is most likely due to the measurement frequency limit as found in other piezoelectric materials [5,10]. The same device was characterized again after two weeks and the piezoelectric response maintained similar (Supplementary Fig. 1). These results demonstrate that the piezoelectric performance of the CNF thin films can be greatly improved by electric poling at room humidity and the induced poling effect remains.

The piezoelectric response of CNF films are found to depend on the humidity of the atmosphere during poling process. In Fig. 1d, CNF thin films poled at four different relative humidity levels (empty columns) are compared with that of non-poled ones (dashed columns) using the same force. The poling of CNF films was performed in a climate chamber with fixed humidity after keeping the samples inside the chamber for 2 hours, and the piezoelectric output voltage was measured in ambient humidity afterwards. Here, we select the samples with the average thickness close to 1μm (±0.1 μm), and then poled them with an increasing voltage between 5 to 110V, and the maximun output votlage is presented in Fig. 1d (corrisponding poling voltage is presented in Supplementary Table 1). The piezoelectric output voltage is

found to be the highest for samples poled in room humidity (40% RH) and smallest values were found from samples poled at high humidity. This might be due to more disociated ions in the samples poled at high humidity that screens the piezoelectric polarization [25]. To prove this, we dried the CNF films poled at 70% RH and then tracked the piezoelectric reponse. As shown in Fig. 1e, the reponse of the same sample increased from 52 mV to 80 mV after drying in low humidity (10% RH) for 30 min.

Electrochemical poling: poling with electrolysis

Electric poling has been successfully applied to enhance the alignment of the electric dipoles in ferroelectric materials, thus improving their piezoelectric performance [26]. However, we did not observe typical ferroelectric poling current as typically found for P(VDF-TrFE) (Supplementary Fig. 2) when sweeping the CNF films with increasing voltage between -110V to 110V (Supplementary Fig. 3). Hence, the CNF film does not exhibit any ferroelectric properties. It should be mentioned that all ferroelectric materials are piezoelectric but the reverse does not apply. Materials having non-centrosymmetric structure could possess piezoelectricity without being ferroelectric [27]. The improved piezoelectric output voltage in poled CNF thin films is likely due to a different mechanism from the ferroelectric PVDFs. As cellulose is known to be hygroscopic with a 10% to 14% water content in the atmospheres carrying a 40% to 50% RH, and as the applied poling voltage exceeds the electrochemical potential for electrolysis of water (1.2 – 2V) [28,29], we assume that electrolysis of water occurs upon poling. In Fig. 2a and 2b, the poling current passing through the CNF film when poled with a linearly increasing voltage at 10% RH and 40% RH were recorded, respectively. Constant scan rate of 5 V s^{-1} was used in all scans and the voltage range was increased for each, from 5 V to 110 V. The non-linear change in current upon applied voltage indicates that it is not capacitive in nature as it would have been expected for dielectric or insulating piezoelectric layers operated below the coercive field. Moreover, the dramatically increasing current with the humidity level of the poling atmosphere suggests that the absorbed water in CNF films undergoes an electrolysis reaction. The decreasing current at the same voltage after each successive scan at low humidity (10% RH) indicates the consumption of water in the film step by step after each scan. The poling current for sample measured under ambient conditions (RH=40%) is high due to the large amount of absorbed water and reabsorption from atmosphere.

To understand the time scale of the water consumption in the CNF film, a constant potential of 30 V is applied to the CNF thin films for 30 s (Fig. 2c), the poling current passing through CNF film during poling is recorded every 5s. For samples measured at all different humidity levels, we observed an exponential decay of the current that tend to stabilize after 25 s. The saturated current for samples poled at high humidity (RH=70%) is 85% of the original value, and the current for samples at low and room humidity decrease to 55% of their original values. Afterwards, the reabsorption of the water from the humid atmosphere is tracked by recording the current while applying a short pulse (t<1s, V=30V) every 50 s. As shown in Fig. 2d, the current increases with the exposure time indicating a regain of water. After 7.5 minutes, the current recovers almost to the same level as before poling for samples exposed at 40% and 70% RH, showing complete regaining of water and equilibrium with the atmosphere. On the contrary, in the dry condition (RH=10%), the normalized current remains at similar level as after poling for the

measured time range, which indicates no obvious water regaining. The recapture of water in the CNF thin films in room humidity after poling is also confirmed by FTIR spectroscopy when the OH vibrational stretching signal is tracked after 30 V poling for 30 s. As shown in Fig. 2e and 2f, the intensity of the OH stretching peak at 3340 cm^{-1} measured at the same location of the CNF film increases with time, and saturates after 10 min. The water content probed by the FTIR signal increases with time due to the water absorption and the FTIR signal evolution follows the measured current evolution in Fig. 2d. The reabsorption of the water after poling, to a level similar found in the CNF films before poling, proves that the change in the piezoelectric property is not due to the water loss from the film.

Morphology changes upon electrochemical poling

We investigated the structural changes of CNF film induced by electrochemical poling at different humidity levels by Atomic Force Microscopy (AFM). To access the surface of the CNF film for probe tip scanning, a separate Au top electrode that can be detached from CNF after poling was designed. As shown in Fig. 3a and 3b, an Au thin film (50 nm of Au on 5 nm of Cr) coated on a PDMS stamp is positioned on the CNF film with slight pressure, which provides a tight and continuous contact with the CNF film and enables effective electric poling (Fig. 3c). After poling at 110V for 30 s at fixed humidity levels (10%, 40% or 70% RH, samples were kept in the humidity for 2 hours before poling), the top electrode was then removed and the surface of the films were characterized with AFM (Fig. 3d). For the samples poled at low humidity (RH =10%), the morphology and phase images (Fig. 3g and 3h) resemble the non-poled films (Fig. 3e and 3f) with only minor change. After poling at room humidity (40% RH), the fibril morphology becomes blurred (Fig. 3i) compared to the non-poled films. In the phase image of the poled CNF layer (Fig. 3j), nano-ring like structures with diameter around 10 nm to 15 nm can be observed. The size of the rings is similar to the diameter of the nanofibrils; which indicates that those rings are the cross section of the fibrils pointing upwards. For films poled at high humidity (70% RH), similar changes can be found with a blur morphology and nano-rings in the phase image (Fig. 3k and 3l). The obvious changes in morphology and phase images after poling at relatively high humidity (> 40%) indicate that the electrochemical poling current leads to the breaking of cellulose nanofibers followed by the reorientation of small segments perpendicular to the surface.

Note that the observed changes do not disappear several month after poling, however, they are not uniform on the whole CNF films. As shown in Supplementary Fig. 4 and 5, different levels of changes can be found on the same sample after poling at relative humidity of 40% and 70%. This could be due to the variation of the CNF films in thickness (up to hundreds of nanometers) resulting in a non-uniform electrochemical current during poling. Indeed, if a hard Au coated glass was used as top electrode, we could never see the morphology/phase changes because of rough CNF films results a poor contact with the flat and hard Au electrode. Moreover, those nano-rings and morphology changes are not found in control experiments. By simply heating those CNF films at 250°C (before thermal degradation) and natural cool down, we could not observe such a change (Supplementary Fig. 6a and 6b). No change in morphology is found by applying the same strength of electric field across a thin air gap as dielectric between the Au top electrode and the CNF film (Supplementary Fig. 6c and 6d). Hence, we believe that the

poling effect in the CNF films is not due to any local Joule heating or electric field, the key mechanism is likely related to “electrochemical poling”, a phenomenon based on electrochemistry and electric field in combination.

The morphology changes in electrochemical poled CNF thin films can be evidenced by the dielectric characterization via impedance spectroscopy (details are discussed in Supplementary Note 2). The typical dynamic phenomena in CNF thin films under a small AC current (from frequency range between 1×10^{-1}- 2×10^{5}) before poling, freshly after poling and 15 hours after poling are compared in Supplementary Fig. 7. The results show obvious changes in the impedance spectroscopy after poling and the change remains similar after 15 hours, which indicate that poling truly leads to an irreversible change of the dielectric properties. The Bode (Supplementary Fig. 8) and Nyquist plot (Supplementary Fig. 9) of the impedance spectroscopy of CNF thin films poled in different humidity further confirmed the role of absorbed water in electrochemical poling and the induced morphology changes.

Piezoelectric device performance

The output voltage (V_{piezo}) of piezoelectric devices depends on the applied force (F), the longitudinal piezoelectric coefficient (d_{33}) and the capacitance (C) of the dielectric material according to:

$$V_{piezo} = \frac{d_{33}F}{C} \qquad (1)$$

We notice that the capacitance at high frequencies (10^{5}- 10^{6} Hz, RH=40%, Supplementary Fig. 8) that is critical for piezoelectric response [30], does not vary after poling at different voltages. Hence, we believe that the piezoelectric voltage measured upon poling is not due to the change in capacitance but mostly an effect of the d_{33} coefficient of the film. Note that the effect of humidity on the capacity value is expected as the introduction of water increases the average dielectric constant of the cellulose layer, however, this effect is vanishingly small (Supplementary Fig. 10). The control experiment of spin-coated CNF thin film also confirms that the structure change of CNF is the key for the enhanced piezoelectric performance instead of water content (details can be found in Supplementary Note 3).

Piezoelectric Force Microscopy (PFM) has been widely used to confirm the reversed piezoelectric effect of a material, as well as to locally measure the piezoelectric coefficient d_{33} (Supplementary Fig. 12a). A DC bias is applied between a conductive AFM tip in contact with the surface of the sample and the substrate, and the deformation of the thin film (in thickness) can be detected by the cantilever. By exploiting PFM technique, we can accurately locate the regions on a CNF thin film that experienced morphology change shown in Fig. 3, measure the d_{33} and compare with that of the regions without visible morphology change. The deflection amplitude of the AFM cantilever (which can be directly correlates to the sample deformation through the deflection sensitivity of the tip, details can be found in experimental section)

with applied bias is presented in Fig. 4. As shown in Fig. 4a, the deformation of region without morphology change is not obvious when applying different bias between the sample and the tip. For effectively poled area as shown in Fig. 4b, the film deformation increases proportionally to the applied bias. The piezoelectric coefficient d_{33} can be calculated from the average linear fitting. As shown in Fig. 4c and 4d, the change of the deflection amplitude of effectively poled area is much larger than the non-effectively poled area of the same sample. The measured average d_{33} is 46 pm V^{-1} for poled areas and only 10 pm V^{-1} for non-poled areas. Same operation of PFM was carried out for poled P(VDF-TrFE) thin films, as shown in Supplementary Fig. 12b, the obtained d_{33} is 46 pm V^{-1}, like previously reported values.

We now compare the piezoelectric performance of the poled CNF thin film devices with that of P(VDF-TrFE) thin films. The linearly increasing piezoelectric voltage with the applied force of poled CNF thin film of the thickness of 0.86 μm and PVDF-TrFE thin film of the thickness of 0.23 μm and 0.55 μm are shown in Supplementary Fig. 13. The similar linear fitting of the output voltage with increasing force for the CNF and P(VDF-TrFE) thin films shows typical piezoelectric response. The thicker P(VDF-TrFE) exhibits higher piezoelectric output voltage than the thin one due to the reduced capacitance. For CNF thin films, the effect of the thickness to achieve optimum piezoelectric output voltage are investigated, and their piezoelectric performance is compared with P(VDF-TrFE) thin films for benchmarking. As shown in Fig. 4e, the piezoelectric response of non-poled CNF films is below 0.03 V when a 24 N force is applied. The response of the two thinnest CNF films is higher than the thicker ones both before and after poling, which seems in opposite trend as for inorganic thin films [31-34]. This could possibly be due to the better alignment of the CNF fibers at the surface of the flat substrate. After poling, the piezoelectric response of CNF films of all thicknesses increased compared to non-poled ones. For samples of thickness between 0.2 to 1 μm, the response of CNF films after poling (with same force of 24 N) increase with the thickness. This is due to the decreasing capacitance with thickness (see Eq. 1), which is also observed for P(VDF-TrFE) thin films (open green squares in Fig. 4e). It is important to note that the piezoelectric output voltage of CNF films is similar to the PVDF based devices in the same conditions. After reaching the maximum value, the piezoelectric output voltage of CNF films starts to decrease with thickness (from 1 to 1.4 μm). This could be attributed to non-effective poling of the thick films. Thin polymer films on a substrate are usually easy to deform under the field due to competing thermodynamic and kinetic factors [35]. The relatively thick CNF films (around 2μm) were also poled with detachable PDMS electrodes, and no change in morphology and phase was then observed. Thick films are more stable than the thin ones since the entangled fibers hinder their reorientation during electric poling; which result in no obvious changes in the morphology and low piezoelectric responses.

In Fig. 4f, the d_{33} of the CNF thin films with different thickness are presented and compared with P(VDF-TrFE). The area capacitance of the P(VDF-TrFE) thin film (0.55 μm) of 13.6 nF cm^{-2} can be obtained from the impedance spectroscopy where the phase angle is close to -90° at high frequency as shown in Supplementary Fig. 15. According to equation (1), the d_{33} of this P(VDF-TrFE) film is 44 pC m^{-1} based on the output voltage in Fig. 4e, which is similar to the PFM values and the previously reported value [36-38]. Note that the unit of the direct and reversed piezoelectric coefficient are different, however they are

equivalent. Though, due to the uneven morphology of the CNF films, it is difficult to obtain the absolute value of the capacitance of those films from the same impedance measurement (detailed discussion can be found in Supplementary Note 4). Hence, we cannot calculate the d_{33} of CNF films in the same way as for P(VDF-TrFE). Instead, previously reported dielectric constant of cellulose (ε_r=10) [39-41] are used to calculate the piezoelectric coefficient of the CNF devices. As shown in Fig. 4f, most of the CNF samples have d_{33} in the range between 35 to 55 pC m^{-1}, which is close to the value obtained from PFM (indicated by the green solid line). We can also see that the effect of electrochemical poling to the piezoelectric performance of CNF thin films depends on the thickness, the maximum improvement of 13 times takes place when the thickness is around 0.7 μm. The results demonstrate that the piezoelectric voltage and d_{33} of electrochemically poled CNF thin films could reach similar value of P(VDF-TrFE) of similar thickness.

Proposed mechanism

As illustrated in Fig. 5a, before poling, CNF fibers composed of alternating amorphous and crystalline regions (enlarged illustration and chemical structures of CNF fiber can be found in Fig. 5d and 5g) are lying relatively parallel to the electrodes. The adsorbed water molecules in the CNF film are mostly bonded to the amorphous region of the cellulose fibers between the crystalline regions (CNC), or on the surface through hydrogen bond with hydroxyl groups [42,43] (the water distribution here). At high level of humidity, water molecules can accumulate between the nanofibers [44]. During the electrochemical poling (Fig. 5b), the ionic conductivity leads to electrochemical reactions as well as perhaps other additional phenomena, such as formation of a space charge polarization like what is found in PVDF films poled in humid environments [45]. The grounded Si electrode is expected to induce half-reaction of O_2 reduction in presence of absorbed water. To describe that in more details, we remind that the oxygen reduction reaction on a non-catalytic surface in neutral environment leads to the production of hydrogen peroxide through the following reduction reaction $O_2 + H_2O + 2e^- \rightarrow HO_2^- + OH^-$ and the acid equilibrium $HO_2^- + H^+ \rightarrow H_2O_2$. Therefore, the neutral environment turns rapidly basic upon this electrochemical reaction. Note that both the basic pH and the H_2O_2 are known to degrade the cellulose [46]. The half-reaction taking place at the positively bias gold electrode could be the oxidation of cellulose (Fig. 5h and 5i) as well as the oxidation of water. Interestingly, the oxidation of cellulose has been reported to be electrocatalytic with Au nanoparticles and on Au electrodes in alkali medium triggering the formation of carbonyl groups on the cellulose that increases its solubility [47,48]. The breaking of the CNF chains into lower molecular weight fractions could also increase the solubility[49]. The formation of carboxylic group in the cellulose film can be evidenced from the growing characteristic C=O peak at 1730 cm^{-1} in Supplementary Fig. 17 obtained after poling at higher voltages. The dissolution of cellulose in the alkali solution is known to promote hydrolysis that cleaves the glycosidic linkage of the polymer chains (Fig. 5i) [50,51]. Further electrocatalytic oxidation paths lead to the formation of gluconate also carrying C=O bonds [47].

Hence, the poling is accompanied with an electrochemical reaction, and that is why we proposed the name “electrochemical poling”. The electrochemical reaction leads to a consumption of the water, and the creation of an alkali medium; which fragilizes the cellulose nanofibrils (Fig. 5e). Finally, the oxidation of cellulose at the gold electrode is promoted by the poling current, which degrades the cellulose by breaking the chains of the biopolymer (Fig. 5f). We believe that the amorphous regions of the nanofibrils, softened by the absorbed water molecules [52], that are in contact with Au become the centers of the electrochemical degradation of the cellulose nanofibrils. As a result, those surface nanofibrils are cleaved at the level of the amorphous regions; and nanocrystals of cellulose are detached. Finally, the high electric field tends to orient preferentially the nanocrystals perpendicular to the Au electrode (Fig. 5c and 5f). The observation of such a surface in the AFM phase images with nano-rings corresponding to the diameter of the fibers supports the hypothesis. Furthermore, grazing incidence small angle x-ray scattering (GISAXS) experiments performed on non-poled and 110V-poled CNF thin films also reveal the poling induced structural changes in these films. As shown in Supplementary Fig. 18, the scattering feature changes observed in the q_z and q_x linecuts, in conjunction with the information derived by AFM, support the hypothesis of a re-orientation of lying-down fibers, with respect to the substrate, towards standing-up fibers upon poling. This electrochemical cleavage of the cellulose nanofibrils is not complete in dry condition (10% RH) due to the lack of absorbed water, hence only partially degraded flat fibers were observed (without total cleavage, Fig. 5e), while nicely oriented nanocrystals are formed at the surface at and above 40% RH (upon total cleavage, Fig. 5f). The new morphology of compact nano-rings at the interface between the CNF bulk and the Au surface is expected to create a new region of different ionic conductivity, this is supposedly the new ionic transport contribution found by impedance spectroscopy (reduced diameter of the first semicircle in Nyquist plot in Supplementary Fig. 9). Indeed, the reorientation of fiber-like fillers perpendicular to the electrode surface has been previously reported to reduce the resistance [53].

Discussion

In this work, we have shown that the electrochemical poling (electric poling in humid environment) is a new method to enhance the piezoelectric coefficient of pure CNF thin films, and the complete device could easily provide an output voltage of 100 mV with 20 N of applied force. For the first time, piezoelectric devices composed of pure nanocellulose are demonstrated with piezoelectric output voltage and piezoelectric coefficient d_{33} similar to PVDF-TrFE based devices. Combining the electrical changes observed from impedance spectroscopy and morphology change in AFM images, we proposed that the improvement of the piezoelectric performance is due to the breaking and re-orientation of the cellulose fibers under electric poling process that induces non centrosymmetric arrangement of the CNC. The humidity level was identified to have important effect on the poling process and affect the result of piezoelectric performance. The investigation of the thickness dependence shows that the electrochemical poling enhancement is only effective for thin CNF films, which limit the output voltage compared to PVDF based devices of scalable thickness. Piezoelectric sensors based on thin films of pure cellulose are sensitive, non-toxic, biodegradable solution processible, scalable on large area. Those features bring

nanocellulose on the map of green and efficient piezoelectric materials with potential impact in self-powered sensing, actuation, wearable and implantable health monitoring etc. with great advantage in wearable and implantable (bio-) electronic applications.

Methods

CNF films and device preparation

Nanofibrillated cellulose (NFC) was produced at Innventia AB, Sweden. 0.5 wt% CNF dispersion in water was used for the thin film fabrication. The CNF are carboxymethylated and has a degree of substitution of 0.1. CNF dispersion in DI water was used to prepare CNF films on doped Si wafers. 0.5 wt% CNF solution was poured dropwise on a Si wafer within a PDMS cavity to define the area of the CNF films. Hence, the average thickness of the CNF film can be tuned by dropping different amount of solution. The films were then dried in an oven at 60°C for 3 h.

For AFM and GISAXS characterizations, the prepared CNF films were directly used as the non-poled samples. To perform the poling, PDMS stamps coated with Cr and Au were used as top electrodes that can be removed after poling. Potentials of 110V was applied between the Au coated PDMS and the doped Si wafer for 30 s at room temperature, the top electrode was removed immediately after poling. For impedance and piezoelectric characterization, the top electrode was fabricated by evaporating Cr (5 nm) and Au (50 nm) directly on the top surface of the CNF films through home-cut plastic shadow mask.

Material characterization

A keithley analyzer (2400) was used to pole the CNF films with different voltage. The impedance measurement was carried out with impedance spectrometer (Alpha high-resolution dielectric analyzer, Novocontrol Technologies GmbH, Hundsangen, Germany) with an AC voltage of 10 mV in the frequency range of 0.1 Hz to 1 MHz. A dimension 3100 was used for the AFM characterization. The images were recorded in tapping mode with tips of 60 kHz resonance frequency. AFM ICON was used for PFM characterization, the Model of the conductive tip is SCM-PIT-V2 with spring constant of 3 N m^{-1} and standard deflection sensitivity of 85 nm V^{-1} (which was calibrated for each measurement).

The thickness of the CNF films was measured by using a surface profiler Dektak3ST (Veeco) across scratches on the films. Roughness of the CNF films were measured by using optical profilometer PLu neox (Sensofar).

The piezoelectric response from the devices were tested at room temperature and recorded with National Instrument (NI) systems. The applied force was controlled by tuning the amplitude of the shaker, and the frequency was maintained 3 Hz. The distance between the probe and the sample surface was kept at 1 mm for all the tests. The effective contact area is 1.13 cm^2. The force was monitored using a force sensor (208C01) placed under the sample. The logging system is NI CDAQ 9174 chassis with NI 9263 voltage output and NI 9239 DAC modules interfaced with a computer using LabVIEW software.

Grazing incidence small-angle x-ray scattering experiments (GISAXS) were performed at the NCD-SWEET beamline of the ALBA Synchrotron, located in Cerdanyola del Vallès, Spain. The wavelength of the X-rays, λ, was 0.9998 Å (12.4 keV), the sample-to-detector distance was 2.538 m and, the angle of incidence, α_i, was set at 0.15°. The diffracted intensity was recorded using a Pilatus 1M Dectris detector. Data were normalized by the incident photon flux and the acquisition time. The scattering vectors in the directions perpendicular and parallel to the substrate, q_z and q_x respectively, are defined as follows: $q_z = 2\pi/\lambda [\sin(\alpha_f) + \sin(\alpha_i)]$ and $q_y = 2\pi/\lambda [\sin(2\theta_f) \cos(\alpha_f)]$, where $2\theta_f$ and α_f are the exit (scattering) angles at the horizontal and vertical directions.

Piezoelectric generator fabrication and characterization

To induce the piezoelectric property in CNF films we poled the films with different poling voltage applied between the top and bottom electrode. At different humidity, the piezoelectric response of the device was recorded first before poling. The poling for each voltage last for 30 s, and afterwards the piezo response was recorded using the same electrical connection as before poling. The piezoelectric response of the poled device was measured directly after the poling finished, and the data was recorded when the signal was stable (the signal is often high at the beginning of the measurement). For the study in high and low humidity levels, the devices were first kept in fixed humidity for 2 hours and the non-poled characterization was carried out in room humidity immediately afterwards. Then the devices were returned to the same humidity for another 2 hours before the poling was conducted in the same humidity. The piezoelectric characterization of poled device was carried out right after poling in room humidity.

Declarations

Acknowledgements

The authors thank the Knut and Alice Wallenberg Foundation (H2O2 and the Wallenberg Wood Science Center), Swedish Research Council (VR 2016-05990, 2016-06146, 2018-04037) as well as the Advanced Functional Materials Center at Linköping University (2009-00971), and finally the NCD-SWEET beamline of ALBA synchrotron in Barcelona, Spain, where X-ray scattering experiments were performed with the collaboration of ALBA staff.

References

1. Miraz, M. H., Ali, M. & Excell, P. S. A Review on Internet of Things (IoT) Internet of Everything (IoE) and Internet of Nano Things (IoNT). *2015 Internet Technologies and Applications, ITA 2015, Proceedings of the 6th International Conference* 219–224 (2015).

2. Liu, J. et.al. Future paper based printed circuit boards for Ggreen electronicsfabrication and life cycle assessment. *Energy Environ. Sci.* **7**, 3674–3682 (2014).

3. Baccarelli, E., Naranjo, P. G. V., Scarpiniti, M., Shojafar, M. & Abawajy, J. H. Fog of everything: energy-efficient networked computing architectures, research challenges, and a case Study. *IEEE Access* **5**, 9882–9910 (2017).

4. Li, X. et al. 3D fiber-based hybrid nanogenerator for energy harvesting and as a self-powered pressure sensor. *ACS Nano* **8**, 10674–10681 (2014).

5. Sultana, A. et al. An effective electrical throughput from PANI supplement ZnS nanorods and PDMS-based flexible piezoelectric nanogenerator for power up portable electronic devices: an alternative of MWCNT filler. *ACS Appl. Mater. Interfaces* **7**, 19091–19097 (2015).

6. Bowen, C. R., Kim, H. A., Weaver, P. M. & Dunn, S. Piezoelectric and ferroelectric materials and structures for energy harvesting applications. *Energy Environ. Sci*. **7**, 25–44 (2014).

7 Briscoe, J. & Dunn, S. Piezoelectric nanogenerators–a review of nanostructured piezoelectric energy harvesters. *Nano Energy* **14**, 15–29 (2015).

8. Ali, W. R. & Prasad, M. Piezoelectric MEMS based acoustic sensors: a review. *Sens. Actuators A* **301**, 111756 (2020).

9. Muralt, P. *Stress Coupled Phenomena:Piezoelectric Effect.* Encyclopedia of Materials: Science and Technology (Elsevier, Oxford, 2001, 8894–8897).

10. Roy, K. et al. A self-powered wearable pressure sensor and pyroelectric breathing sensor based on GO interfaced PVDF nanofibers. *ACS Appl. Nano Mater*. **2**, 2013–2025 (2019).

11. Shepelin, N. A. et al. Interfacial piezoelectric polarization locking in printable $Ti_3C_2T_x$ MXene-fluoropolymer composites. *Nat. Commun*. **12**, 3171 (2021).

12. Zulfiqar, S., Zulfiqar, M., Rizvi, M. & Munirt, A. Study of the thermal degradation of polychlorotrifluoroethylene, poly(vinylidene fluoride) and copolymers of chiorotrifluoroethylene and vinylidene fluoride. *Polym. Degrad. Stab*. **43**, 423–430 (1994).

13. Sencadas, V. et al. Electroactive properties of electrospun silk fibroin for energy harvesting applications. *Nano Energy* **66**, 104106 (2019).

14. Bazhenov, V. A. *Piezoelectric Properties of Woods* (Consultants Bureau: New York, 1961).

15. Fukada, E. Piezoelectricity as a fundamental property of wood. *Wood Sci. Technol*. **2**, 299–307 (1968).

16. Song, Y. et al. Recent advances in cellulose-based piezoelectric and triboelectric nanogenerators for energy harvesting: a review. *J. Mater. Chem. A* **9**, 1910–1937 (2021).

17. Chae, I., Jeong, C. K., Ounaies, Z. & Kim, S. H. Review on electromechanical coupling properties of biomaterials. *ACS Appl. Bio Mater*. **1**, 936–953 (2018).

18. Fukada, E. History and recent progress in piezoelectric polymers. *IEEE Trans. Ultrason. Ferroelectr. Freq. Control* **47**, 1277–1290 (2000).

19. Rajala, S. Cellulose nanofibril film as a piezoelectric sensor material. *ACS Appl. Mater. Interfaces* **8**, 15607–15614 (2016).

20. Zhai, L., Kim, H. C., Kim, J. W. & Kim, J. Alignment effect on the piezoelectric properties of ultrathin cellulose nanofiber films. *ACS Appl. Bio Mater*. **3**, 4329–4334 (2020).

21. Wang, J. et al. Piezoelectric nanocellulose thin film with large-scale vertical crystal alignment. *ACS Appl. Mater. Interfaces* **12**, 26399–26404 (2020).

22. Frka-Petesic, B., Jean, B. & Heux, L. First experimental evidence of a giant permanent electric-dipole moment in cellulose nanocrystals. *EPL Europhysics Lett*. **107**, 28006 (2014).

23. Håkansson, K. M. O. et al. Hydrodynamic alignment and assembly of nanofibrils resulting in strong cellulose filaments. *Nat. Commun*. **5**, 4018 (2014).

24. Wise, H. G., Takana, H., Ohuchi, F. & Dichiara, A. B. Field-assisted alignment of cellulose nanofibrils in a continuous flow-focusing system. *ACS Appl. Mater. Interfaces* **12**, 28568–28575 (2020).

25. Sultana, A., Alam, M. M., Fabiano, S., Crispin, X. & Zhao, D. Enhanced ionic transport in ferroelectric polymer fiber mats. *J. Mater. Chem. A* **9**, 22418–22427 (2021).

26. McGinn, C. K. et al. Formulation, printing, and poling method for piezoelectric films based on PVDF–TrFE. *J. Appl. Phys*. **128**, 225304 (2020).

27. Kholkin, A. L., Pertsev, N. A. & Goltsev, A. V. *Piezoelectricity and Crystal Symmetry*. In: Safari A., Akdoğan E.K. (eds) Piezoelectric and Acoustic Materials for Transducer Applications (Springer, Boston, MA, 2008).

28. Penttilä, P. A. et al. Moisture-related changes in the nanostructure of woods studied with X-ray and neutron scattering. *Cellulose* **27**, 71–87 (2020).

29. Garg, M. et al. Moisture uptake in nanocellulose: the effects of relative humidity, temperature and degree of crystallinity. *Cellulose* **28**, 9007–9021 (2021).

30. Darestani, M. T., Chilcott, T. C. & Coster, H. G. L. Electrical impedance spectroscopy study of piezoelectric PVDF membranes. *J. Solid State Electrochem*. **18**, 595–605 (2014).

31. Nguyen, M. D., Dekkers, M., Vu, H. N. & Rijnders, G. Film-thickness and composition dependence of epitaxial thin-film PZT-based mass-sensors. *Sens. Actuators A* **199**, 98–105 (2013).

32. Nguyen, M. D., Houwman, E. P. & Rijnders, G. Large piezoelectric strain with ultra-low strain hysteresis in highly *c*-axis oriented $Pb(Zr_{0.52}Ti_{0.48})O_3$ films with columnar growth on

amorphous glass substrates. *Sci. Rep*. **7**, 12915 (2017).

33. Kim, D. M. et al. Thickness dependence of structural and piezoelectric properties of epitaxial $Pb(Zr_{0.52}Ti_{0.48})O_3$ films on Si and $SrTiO_3$ substrates. *Appl. Phys. Lett*. **88**, 142904 (2006).

34. Li, J. F., Zhu, Z. X. & Lai, F. P. Thickness-dependent phase transition and piezoelectric response in textured Nb-doped $Pb(Zr_{0.52}Ti_{0.48})O_3$ thin films. *J. Phys. Chem. C* **114**, 17796–17801 (2010).

35. Forrest, J. A., Dalnoki-Veress, K. & Dutcher, J. R. Interface and chain confinement effects on the glass transition temperature of thin polymer films. *Phys. Rev. E* **56**, 5705–5716 (1997).

36. Omote, K., Ohigashi, H. & Koga, K. Temperature dependence of elastic, dielectric, and piezoelectric properties of “single crystalline” films of vinylidene fluoride trifluoroethylene

copolymer. *J. Appl. Phys*. **81**, 2760–2769 (1997).

37. Choi, Y. Y. et al. Vertically aligned P(VDF-TrFE) core-shell structures on flexible pillar arrays. *Sci. Rep*. **5**, 10728 (2015).

38. Jia, N., He, Q., Sun, J., Xia, G. & Song, R. Crystallization behavior and electroactive properties of PVDF, P(VDFTrFE) and their blend films. *Polym. Test*. **57**, 302–306 (2017).

39. Tao, J., Jiao, L. & Deng, Y. *Cellulose and Nanocellulose Based Dielectric Materials Ch. 4,* (Micro and Nano Technologies, Nanocellulose Based Composites for Electronics, 2021, 73–100).

40. Kadimi, A., Benhamou, K., Habibi, Y., Ounaies, Z. & Kaddami, H. *Nanocellulose Alignment and Electrical Properties Improvement, Multifunctional Polymeric Nanocomposites Based on Cellulosic Reinforcements Ch. 11*, (William Andrew Publishing, 2016, 343–376).

41. Tao, J. & Cao, S. Flexible high dielectric thin films based on cellulose nanofibrils and acid oxidized multi-walled carbon nanotubes. *RSC Adv*. **10**, 10799–10805 (2020).

42. Guo, X., Wu, Y. & Xie, X. Water vapor sorption properties of cellulose nanocrystals and

nanofibers using dynamic vapor sorption apparatus. *Sci. Rep*. **7**, 14207 (2017).

43. Lundahl, M. J. Strength and water interactions of cellulose I filaments wet-spun from cellulose nanofibril hydrogels. *Sci. Rep*. **6**, 30695 (2016).

44. Kalkavoura, V. A. et al. Humidity-dependent thermal boundary conductance controls heat transport of super-insulating nanofibrillar foams. *Matter* **4**, 276–289 (2021).

45. Martin, B., Vizdrik, G. & Kliem, H. Influence of the relative humidity on the properties of ferroelectric poly(vinylidene fluoride-trifluoroethylene). *J. Appl. Phys*. **105**, 084114 (2009).

46. Brooks, R. E. & Moore, S. B. Alkaline hydrogen peroxide bleaching of cellulose. Cellulose 7, 263–286 (2000).

47. Xiao, H., Wu, M. & Zhao, G. Electrocatalytic oxidation of cellulose to gluconate on carbon aerogel supported gold nanoparticles anode in alkaline medium. *Catalysts* **6**, 5 (2016).

48. Matsumoto, F., Harada, M., Koura, N., Idemoto, Y. & Ui, K. Enhancement of electrochemical oxidation of glucose at Hg Adatom-modified Au electrode in alkaline aqueous solutions. *Electrochemistry* **72**, 103–110 (2004).

49. Sugano, Y., Latonen, R.-M., Pirkanniemi, M. A., Bobacka, J. & Ivaska, A. Electrocatalytic oxidation of cellulose at a gold electrode. *ChemSusChem*. **7**, 2240–2247 (2014).

50. Biermann, C. J. Hydrolysis and other cleavages of glycosidic linkages in polysaccharides. *Adv. Carbohydr. Chem. Biochem*. **46**, 251–271 (1988).

51. Knill, C. J. & Kennedy, J. F. Degradation of cellulose under alkaline conditions. *Carbohydr. Polym*. **51**, 281–300 (2003).

52. Aulin, C., Gällstedt, M. & Lindström, T. Oxygen and oil barrier properties of microfibrillated cellulose films and coatings. *Cellulose* **17**, 559–574 (2010).

53. Mason, T.O., Campo, M.A., Hixson, A. D. & Woo, L.Y. Impedance spectroscopy of fiber-reinforced cement composites. *Cem. Concr. Compos*. **24**, 457–465 (2002).

Figures

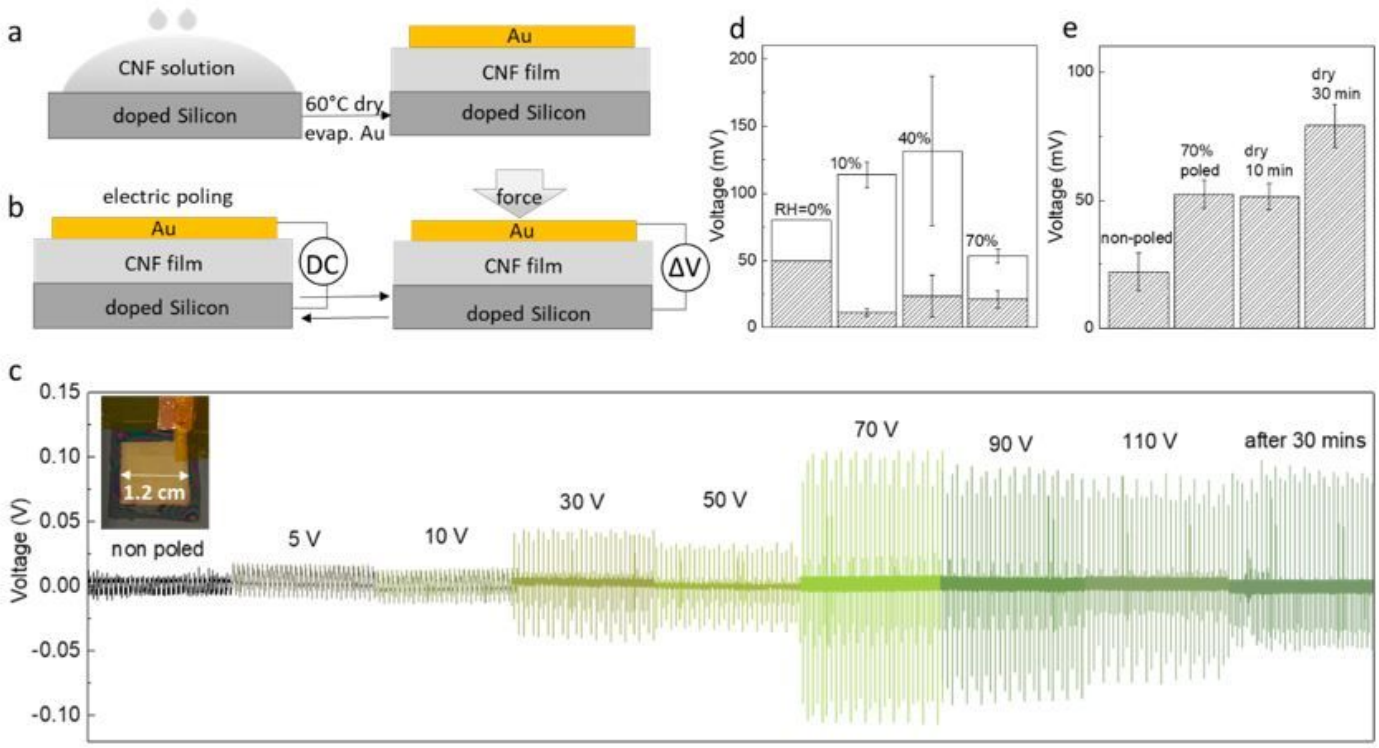

Figure 1

Demonstration of poling induced piezoelectric enhancement in CNF thin films. (a) Schematic illustration of the preparation of CNF thin film-based piezoelectric devices. (b) Poling and piezoelectric measurement of the CNF based devices. (c) Piezoelectric response of CNF film with increasing poling voltage, with constant applied force (24 N) at 3 Hz frequency. The effective area of the device is 1.13 cm^2 where the force is applied. Inset shows the photograph and dimension of a CNF thin film-based piezoelectric device. (d) The piezoelectric output voltage of the CNF films before and after poling at different humidity. The error bars correspond to the standard deviation between 3-5 different samples. (e) The piezoelectric output voltage for CNF samples poled a 70% RH before and after drying in low humidity (10% RH). The error bars correspond to the distribution of the output voltage of the same sample in a measurement period of 20s.

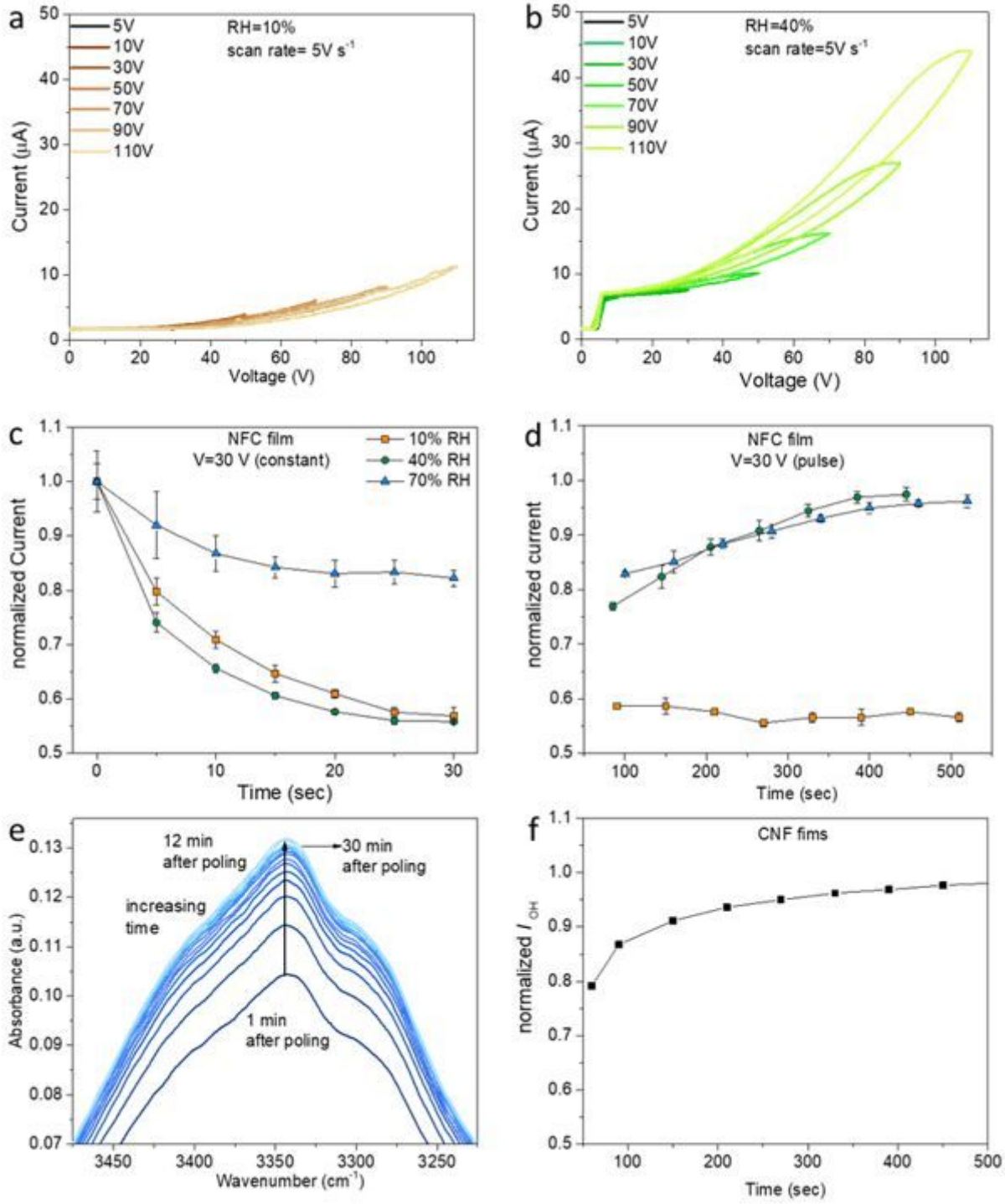

Figure 2

The impact of water in the poling process. The poling current-voltage characteristics (cyclic voltammogram) of CNF devices at (a) 10% RH and (b) 40% RH (scan rate = 5 V s^{-1}). Normalized current (compare to the current at the beginning of the poling) change with time (c) while losing water from CNF film under constant applied voltage of 30V and (d) while regaining water. The current was recorded by applying pulse voltage of 30V. e) The increasing OH stretching peak of CNF thin film after poling with 30

V for 30s. f) The normalized intensity of the OH stretching peak changing with time. The error bar corresponds to 3 times of measurements of the same sample.

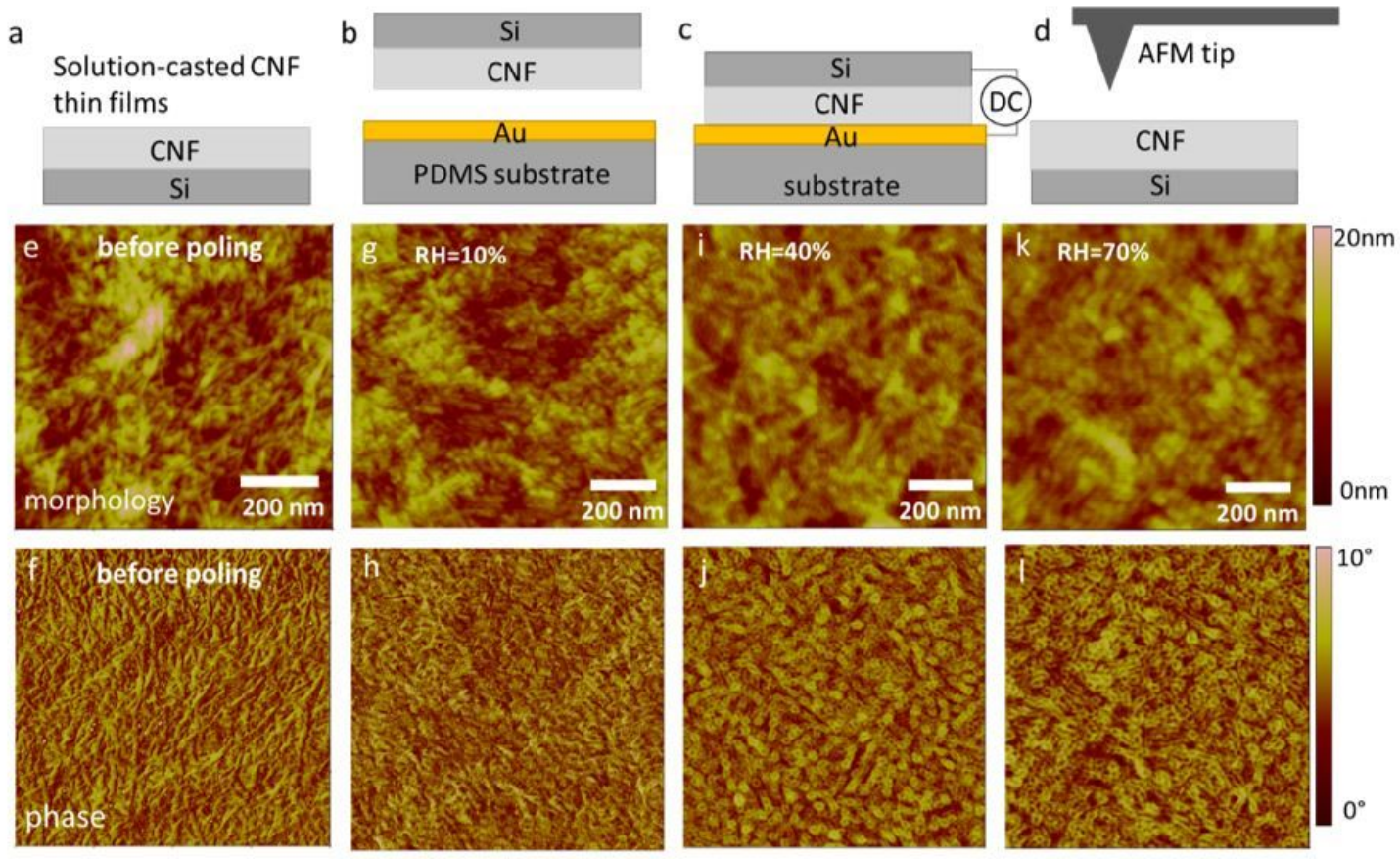

Figure 3

AFM characterization of CNF thin films before and after poled at different humidity. (a) Preparation for CNF film. (b and c) Electrical poling of CNF film (110 V) with detachable soft electrode. (d) Illustration of the AFM characterization of the surface of CNF thin films. Morphology and phase characterization of CNF thin film before poling (e and f), poled at RH=10% (g and h), RH=40% (i and j) and RH=70% (k and l).

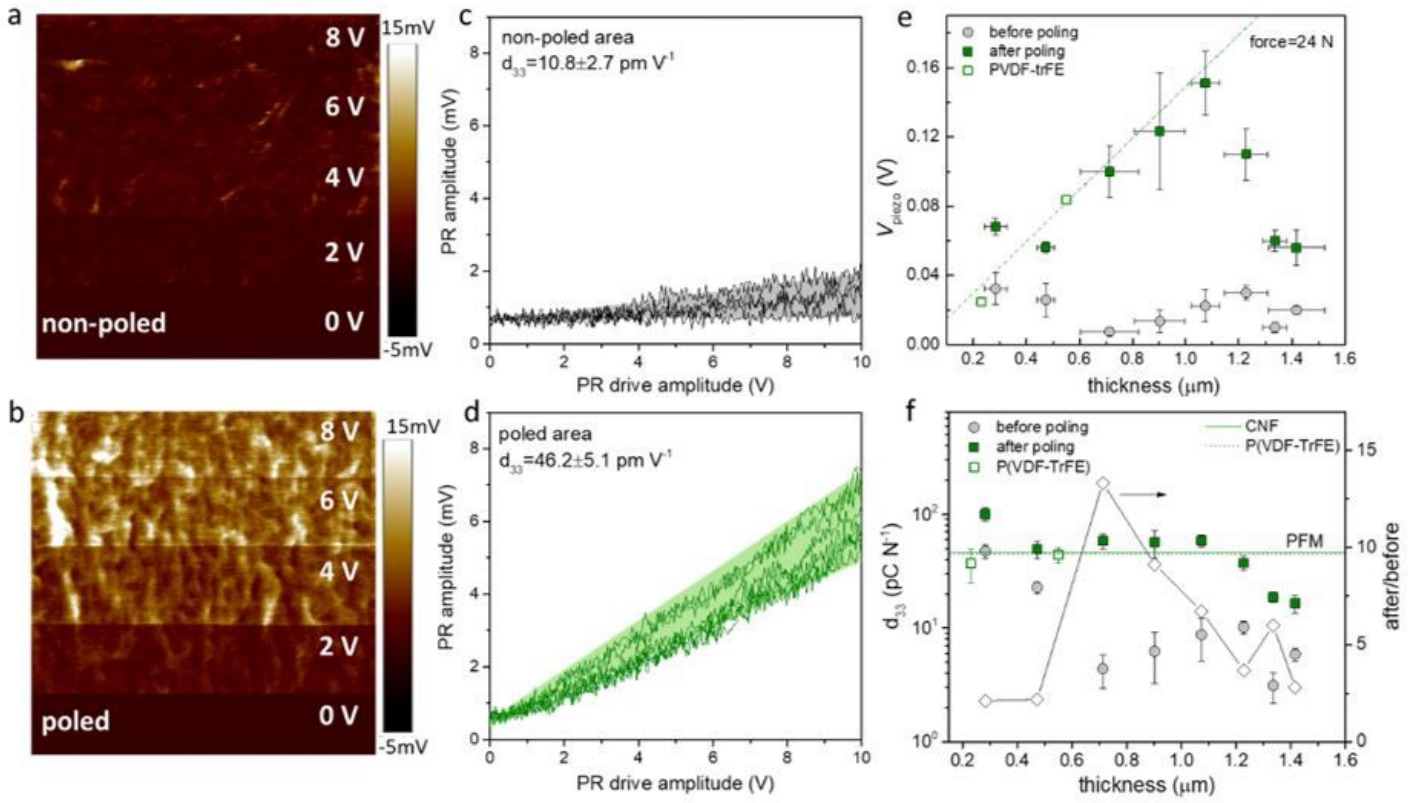

Figure 4

Piezoelectric coefficient and performance of CNF thin films. The deflection amplitude under different bias for non-effectively poled (a) and poled regions (b) of CNF thin film. The spectroscopy of the deflection amplitude changes with increasing applied bias at non-effectively poled (c) and poled regions (d). 5 spots were measured for non-poled regions and 10 spots were measured for poled areas. (e) Thickness dependent piezoelectric response of CNF and P(VDF-TrFE) thin films before and after poling. The dash line indicates the calculated piezoelectric response of P(VDF-TrFE) with increasing thickness under the same force condition. (f) The piezoelectric coefficient d_{33} and the ratio of the piezoelectric output voltage of CNF films before and after poling. The error bar is the standard deviation from the 3 to 5 samples at each thickness range. The same force of 24N, 3 Hz was used.

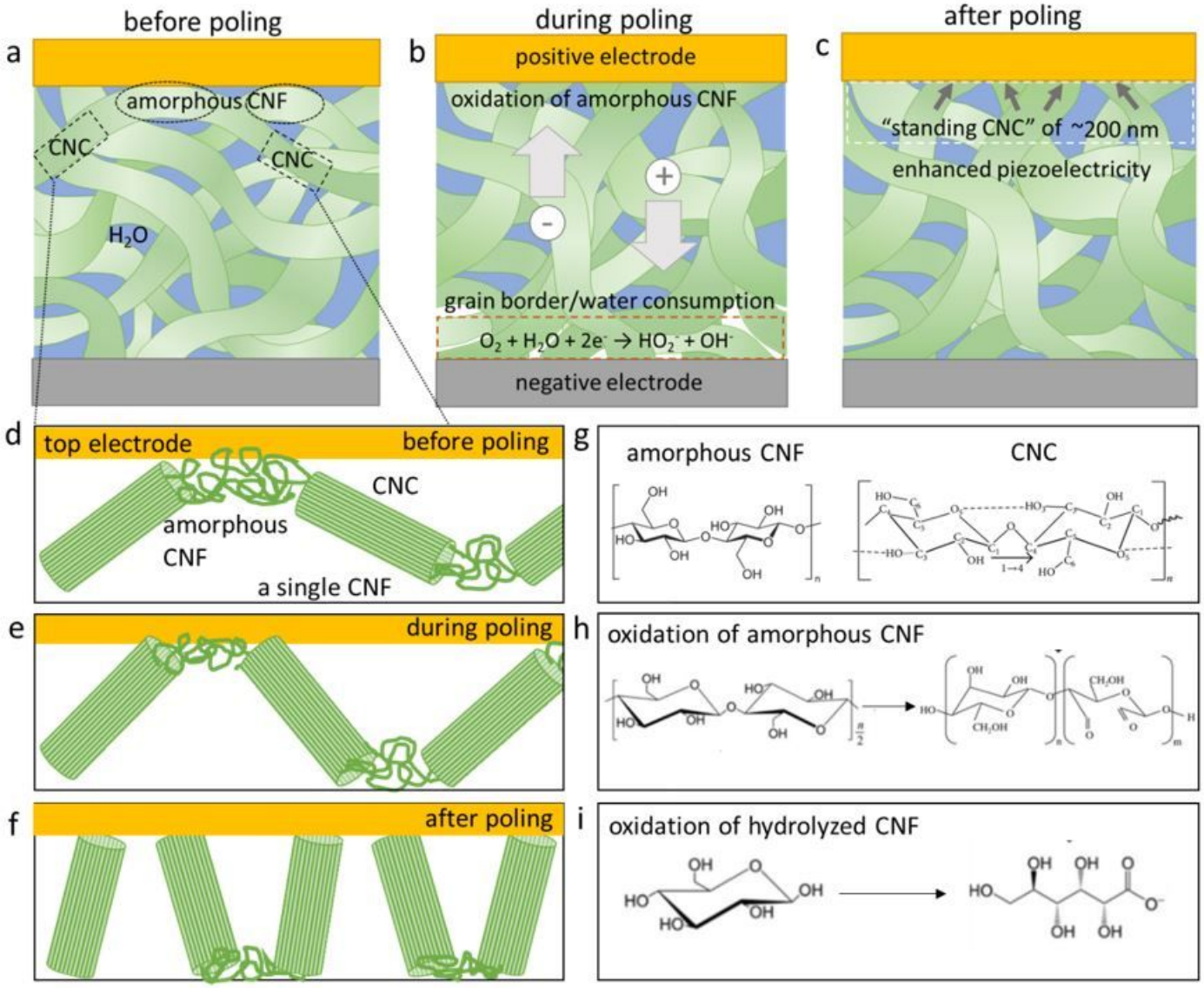

Figure 5

Illustration of the possible changes in CNF thin films during elecrochemical poling. The structure of CNF film before (a), during (b) and after (c) electrochemical poling. The structure of a single CNF that is close to the top Au electrode before poling (d), during poling (e) and after poling (f). For CNF films poled at low humidity, the change might stop at (e). The chemical structures of CNF (g) and reactions for oxidation of CNF (h and i).

Supplementary Files

This is a list of supplementary files associated with this preprint. Click to download.

- SupplementaryImformation.docx